Electronic Supplementary Material (ESI) for Nanoscale.

Supporting Information

Deformable and Wearable Carbon Nanotube Microwires-based Sensors for Ultrasensitive Monitoring of Strain, Pressure and Torsion

Jian Zhou,*,† Xuezhu Xu,† Hu Yu,‡ and Gilles Lubineau*,†

E-mail: jian.zhou@kaust.edu.sa; gilles.lubineau@kaust.edu.sa

This PDF file includes:

*To whom correspondence should be addressed

†King Abdullah University of Science and Technology (KAUST), Physical Sciences and Engineering Division, COHMAS Laboratory, Thuwal 23955-6900, Saudi Arabia; Tel:+966(12)8082983

‡Shanghai Jiao Tong University, School of Mechanical Engineering, State Key Laboratory of Mechanical Systems and Vibration, 800 Dongchuan Road, Minhang District, Shanghai, 200240, P.R.China

1. Fabrication and sample information

Table S1. Summary of the sample information in this study

Sample name	Abbreviation	Needle gauge	wire width	Resistance (Ω cm^{-1})
Large SWCNT wire in PDMS	60-μm-SWCNT	23 G	60±8	90±10
Small SWCNT wire in PDMS	32-μm-SWCNT	34 G	32±4	2500±200

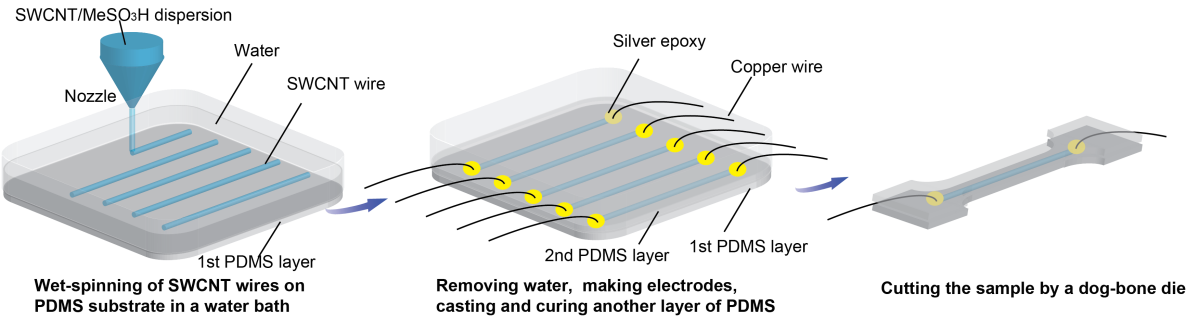

Figure S1. Key steps in fabrication of PDMS-encapsulated SWCNT wire mechanical sensor.

We monitored the first fragmentation process on a 60μm-SWCNT sample by applying strain and relaxation (0 to 50 % and 50 to 0%). Figure. S2b presents the changes in resistance of the sample as a function of time. During this process, the number and size of cracks increased with strain, but the resistance did not change continuously due to the propagation of the cracks. In detail, the resistance remained 336 Ω before $\varepsilon < 4\%$. The resistance increased from 336 to 751 Ω when the first crack appeared at a strain of 5%. It is important to know that the crack opening distance is roughly 10 μm and 100 μm at strains of 5% and 10%, respectively, indicating that SWCNT bundles and networks exist in the same crack. Then, the resistance increased to infinity at a strain of 15%, indicating that the SWCNT networks in the cracks were completely disconnected. At a strain of 50%, seven cracks appeared in the wire. During the relaxation process, we found that the cracks gradually disappeared by decreasing the strain from 50% to 0%. The final resistance after relaxation was almost equal to the initial resistance (Figure S2d).

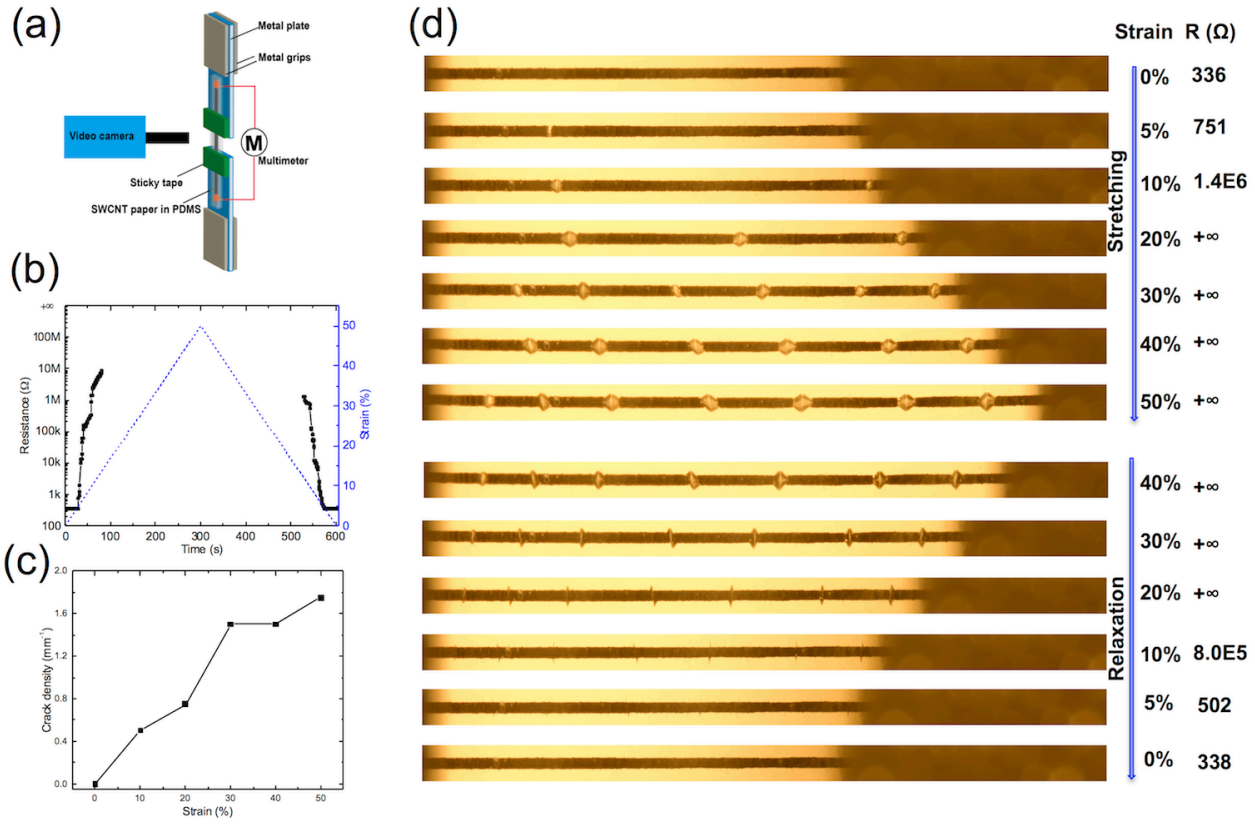

Figure S2. Fragmentation of SWCNT wire in PDMS. (a) The setup for sample fragmentation and the electromechanical test. (b) Change in resistance and strain with time during fragmentation. (c) Change in crack density with strain during fragmentation. (d) Optical images of SWCNT wire in PDMS during the stretching and relaxation process.

2. Characterization of SWCNT fibers

Self-standing SWCNT fibers were also prepared to estimate the mechanical properties of the SWCNT wires. The spinning formulation was loaded into a 5 mL plastic syringe and spun into a water coagulation bath though a 34 G metal needle. The flow rate of the ink was controlled to 20 μL min^{-1} by using a syringe pump. The fibers were collected vertically onto a 50 mm winding spool, which had a linear velocity of 2 to 4 m min^{-1}. The air temperature along the path of the fiber was controlled to 90 °C by two vertically located hot-plates. The temperature was monitored by a thermocouple.[1]

The mechanical behavior of the fibers was measured by a 5944 Instron universal testing machine at a strain rate of 0.4 mm min^{-1}. The tests were performed inside an enclosure to protect

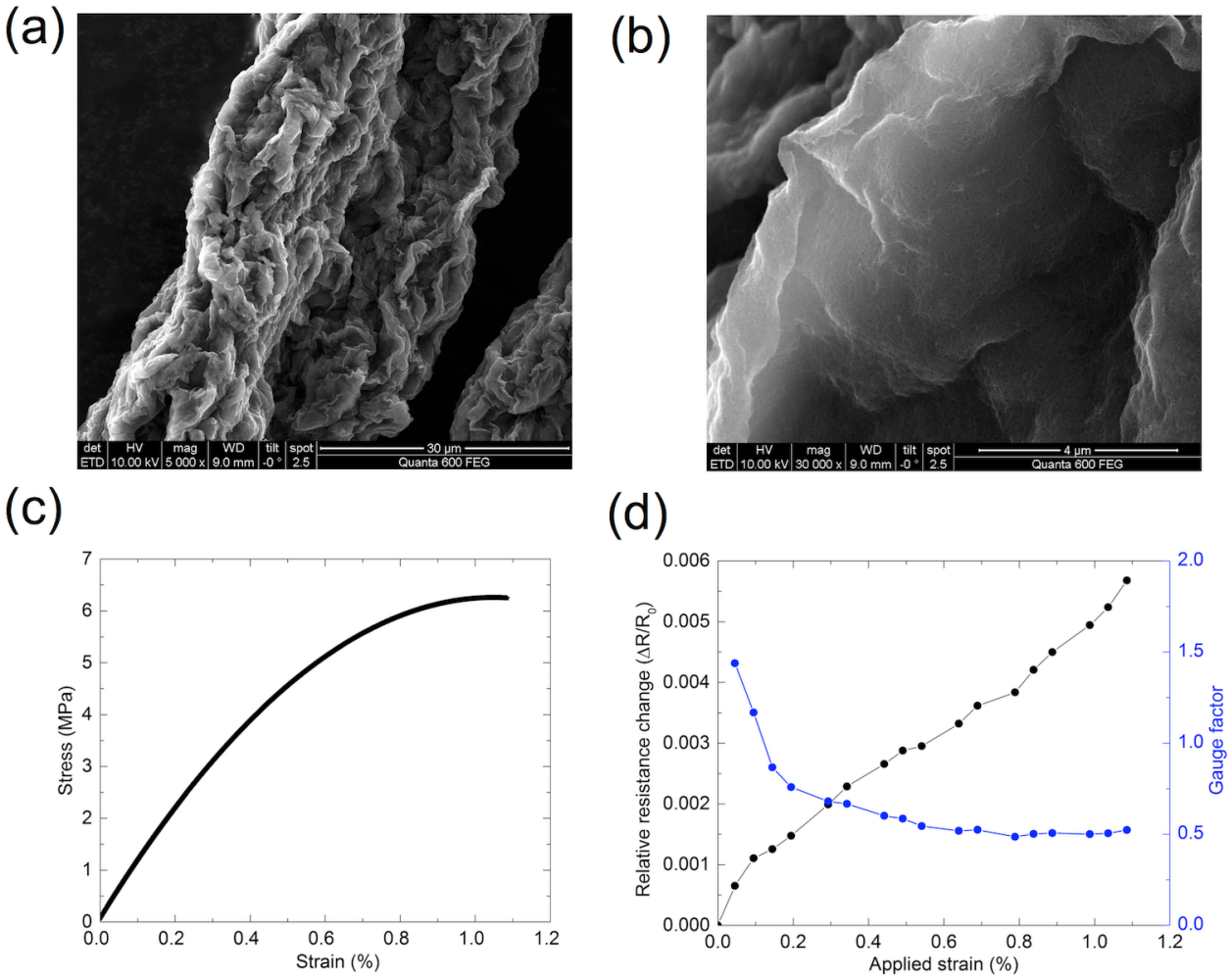

Figure S3. Characterization of SWCNT fibers. (a) and (b) SEM images at different magnifications. (c) A typical stress-strain curve of a SWCNT fiber. (d) Relative resistance change and gauge factor versus applied strain of a SWCNT fiber.

the fibers from environmental disturbances. 2-cm-long fibers were prepared and fixed on a paper card. The average values of tensile strength, Young's modulus and elongation were based on measurements from at least 10 samples.

3. Comparison study based on carbon fibers

We understood that fragmentation allowed the SWCNT wires to achieve high sensitivity in PDMS compared with other CNT-based strain sensors. With the help of PDMS, the resistance of the wire

has excellent reversibility after relaxation. It is important to point out the our SWCNT wires in PDMS has a very low stiffness (0.77 GPa) compared with similar studies in literature. Moreover, the SWCNT wire has a very rough surface which increases adhesion with PDMS. To support our analysis, we replaced the SWCNT wire with a smooth carbon fiber (diameter: 7μm) and encapsulated it with PDMS using the same encapsulation method. Figure S4a shows that the resistance of the carbon fiber increased from 9800 to nearly 10,000 at a strain of 2.5% and it experienced irreversible mechanical and electrical failure. The carbon fiber pulled away from the PDMS and obvious de-bonding can be observed. The break point of a carbon fiber cannot reconnected like it can be in SWCNT wires even after a 20 min rest (Figure S4b). This is because the high stiffness of the carbon fiber with respect to the PDMS resulted in the development of only one crack, which reduced the elongation at the break and the cracked surface could not perfectly matched during unloading, which prevented recovery of the electrical properties.

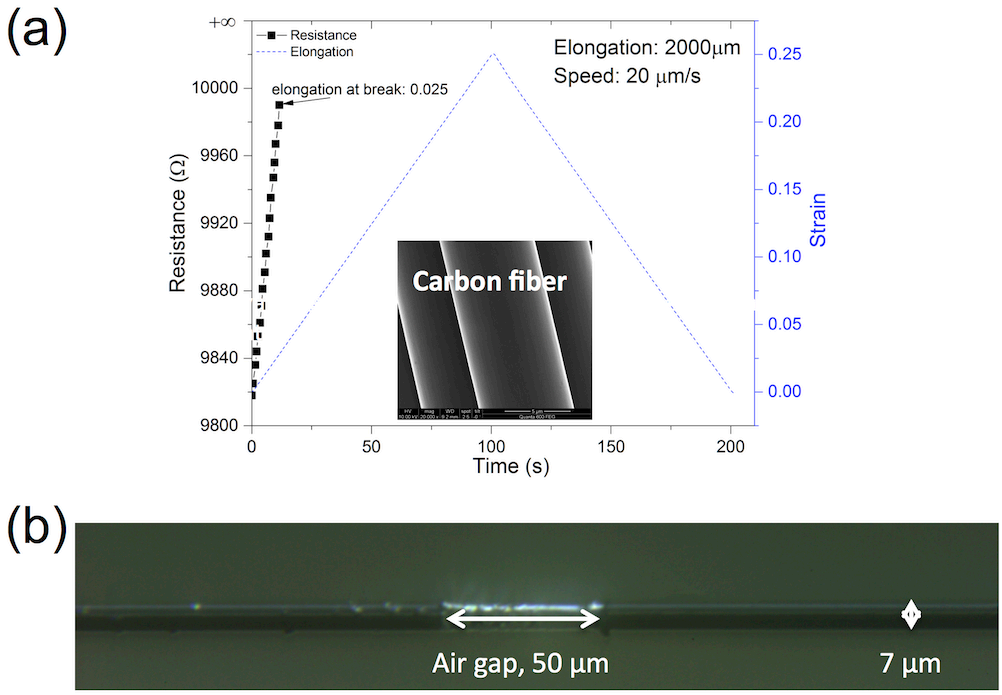

Figure S4. Electromechanical response of a carbon fiber in PDMS.

4. Additional characterization based on SWCNT wire mechanosensors

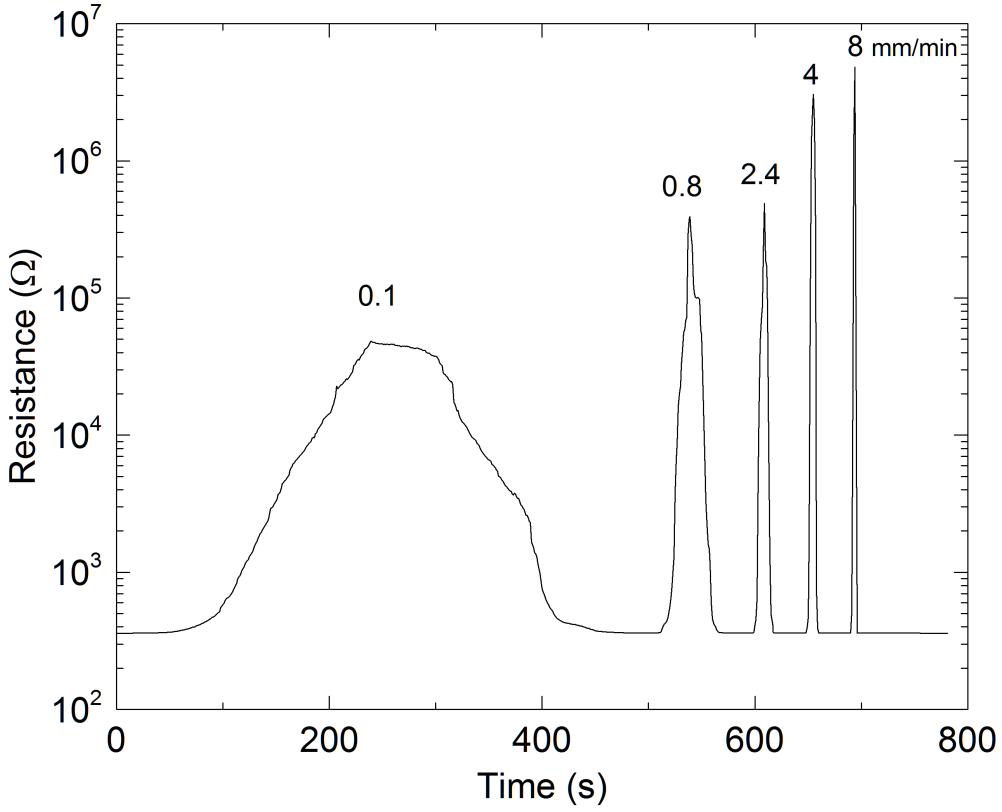

Figure S5. Resistance change of SWCNT wire during cyclic loading at different speed of 0.1, 0.8, 2.4, 4 and 8 mm min^{-1}

The electrical properties of the sample after large mechanical deformation were further demonstrated in a electrical circuit, in which the sample was connected to a 3 V battery and a LED (Figure S6). At the initial state, the LED lit up, indicating that SWCNT wires can be used as interconnects in the circuit. During stretching to 50 or 100% of strain, we observe that the LED goes off, confirming the fragmentation of the SWCNT wire at large strain. After relaxation from 50 or 100% strain, the LED automatically turns back on, proving that the open circuit was connected due to the automatic recovery of resistance after relaxation. The remarkable resistance recovery properties after fragmentation come from the good adhesion of the SWCNT wire with PDMS due to an excel-

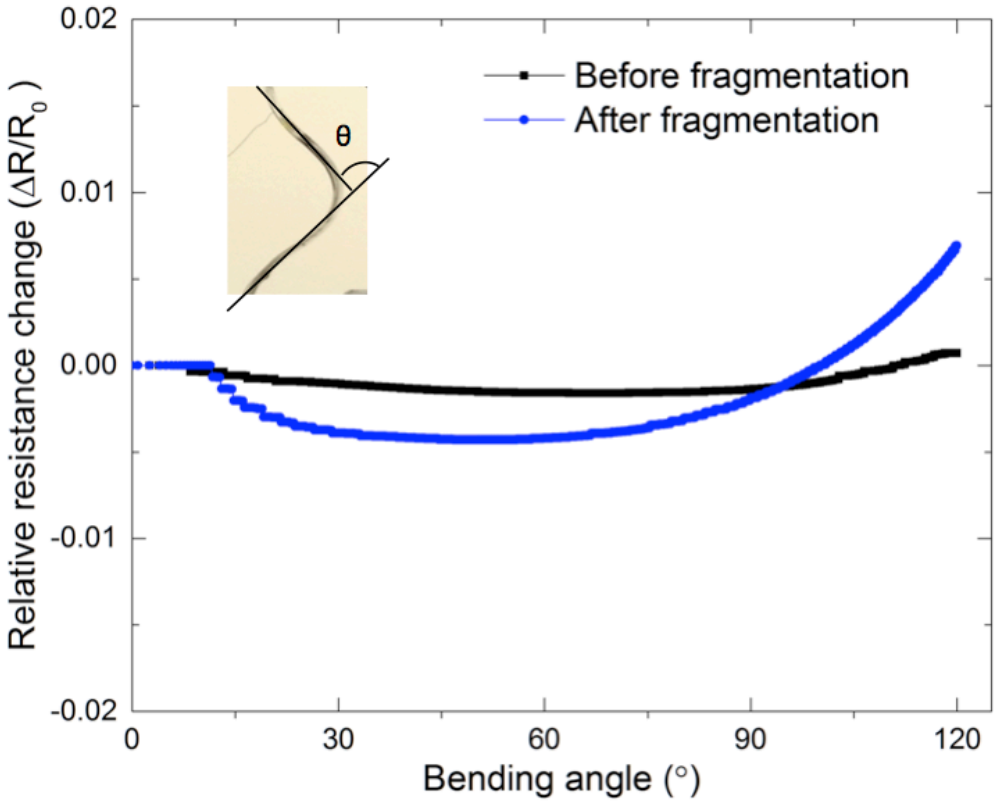

Figure S6. Relative resistance change vs bending angle of SWCNT wire before and after fragmentation using the method in Figure 1a. The insert shows an image of definition of the bending angle θ.

lent capillary surface of SWCNT. Therefore, by immersing the SWCNT wires in PDMS precursor, the PDMS becomes firmly attached to the SWCNT wire. In addition, PDMS is inherently self-recoverable, such that it brings the CNT networks back to the original location. The low stiffness of SWCNT wire makes it easily fragmented. The resistance recovery characteristics enable us to use the sensor in stretchable electronics, which can have the additional functionality of recovery after larger strain up to 100%.

Table S2. Summary of strain sensing properties based on previously reported nanomaterial-enabled stretchable conductors.

Materials	Initial electrical properties (R_0)	$\Delta R/R_0$	Maximum strain	Gauge factor	Ref.
CNT yarn	$R_0^{a)}$=3.4 kΩ	0.016	3.5%	0.45	[2]
Random SWCNT film on PDMS	$\sigma^{b)}$ =2200 Scm^{-1}	5	150%	3.4	[3]
Random MWCNT film in Ecoflex		2.5	100 %	1	?
Thickness gradient SWCNT film on PDMS	σ =2200 Scm^{-1}	3.2	2 %	161	[4]
Aligned SWCNT film on PDMS	-	3.28	40%	0.82	[5]
Aligned SWCNT film on PDMS	-	0.12	200%	0.06	[5]
3D SWCNT network in PDMS	-	0.35	1%	35	[6]
(PU-PEDOT/PSS)/SWCNT/(PU-PEDOT:PSS) on a PDMS	-	62	100%	62	[7]
Aligned mico/nano carbon particles in PDMS	$R_s^{c)}$ = 60 Ω $\square^{-1}$	20000	100%	20000	[8]
CNT fiber on prestrained Ecoflex substrate	σ = 0.257 Scm^{-1}	358	960%	64	[9]
AgNW film in PDMS	R_0 = 7.5-246 Ω	9.8	70%	14	[10]
AgNW arrays in pre-strained PDMS	R_0 = 5.3 Ω	7	35%	20	[11]
Graphene on PE fiber in PDMS	σ = 0.012-0.136 Scm^{-1}	1.8	50%	3.7	[12]
Graphene foam on PDMS	R_0 = 1000 Ω	30	70%	29	[13]
Graphene on PET	R_0 = 15 kΩ	0.8	2%	15	[13]
Nanoscale crack based metal/Polyurethane acrylate	-	35	2%	6	[14]
SWCNT wire in PDMS	R = 368 Ω or 10 kΩ	5×10^4	15%	10^5	This study

[a)]initial resistance, [b)]electrical conductivity, and [c)]sheet resistance

Table S3. Summary of sensing properties to multiple deformation modes based on previously reported nanomaterial-enabled mechanical sensors

Materials	Gauge factor at ε_m	Pressure sensitivity at P_m	Torion sensitivity at ϕ_m	Bending sensitivity at θ_m	Ref.
Random SWCNT film on PDMS	3.4 at 150%	0.22 MPa^{-1} at 0.9 MPa	-	-	[3]
Interlocking of Pt-coated nanofibers		11.5 at 0.5 MPa	8.53 at 0.002 N m		[15]
Cracked silver nanoparticle film on PDMS	2.1 at 20%	200 MPa^{-1} at 3kPa	-	-	[16]
Pencil trace on paper	536.6 at 0.6 %	GF=150.5 at -0.6%	-	-	[17]
Graphene-based fiber	1.5 at 200%		1.2/800rad/m at 800rad/m	0.003 deg^{-1} at 90 deg	[12]
AgNW coated fabric with stretchable sensor arrays	0.7 at 100%	0.45 N^{-1} at 2N	-	0.0133 deg^{-1} at 60 deg	[18]
SWCNT wire in PDMS	30000 at 15%	40000 MPa^{-1} at 0.8MPa	-	10^{-4} $degree^{-1}$ at 120 degree	This study

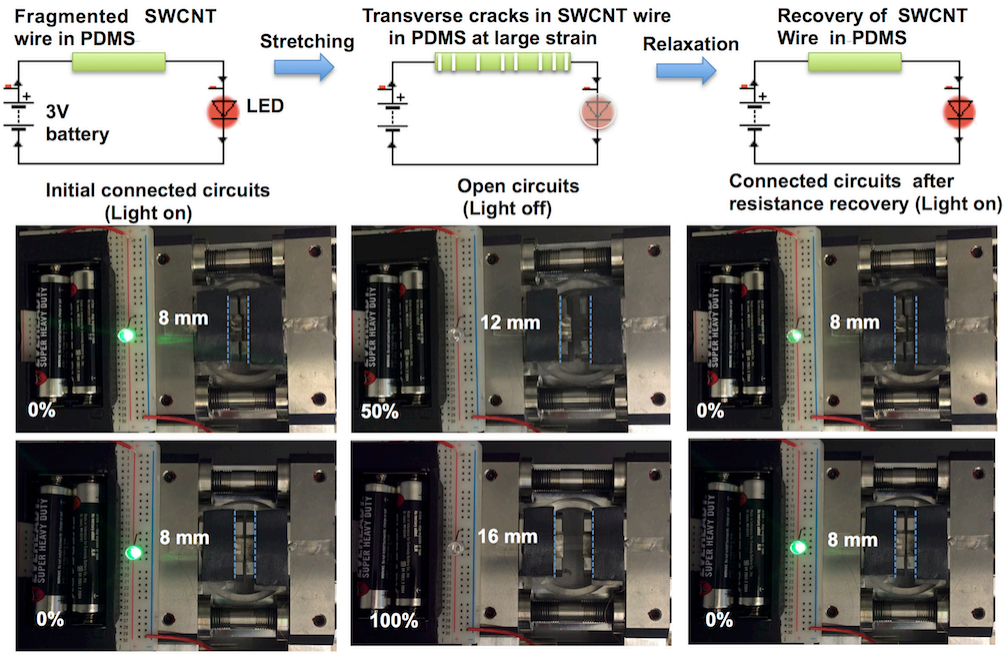

Figure S7. Demonstration of resistance recovery process of fragmented SWCNT wires in electronic circuit. The SWCNT wire was stretched to 50% and 100%, which is beyond the limit of the maximum strain at 15%. The resistance of the wire can recover and lit up an LED.

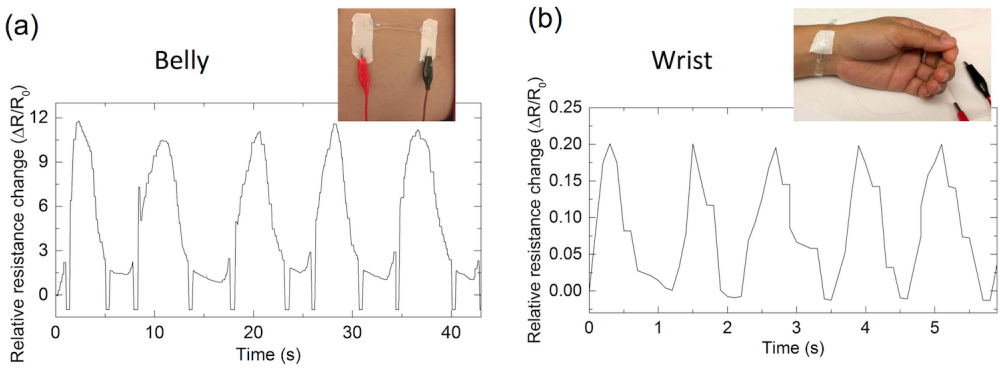

Figure S8. The sensor's response to small mechanical deformations in human motion detection. (a) The motion-dependent response of the sensor attached the belly. (b)The motion-dependent response of the sensor attached the artery of the wrist.

References

(1) Zhou, J.; Li, E. Q.; Li, R.; Xu, X.; Aguilar Ventura, I.; Moussawi, A.; Anjum, D.; Hedhili, M. N.; Smilgies, D.; Lubineau, G.; Thoroddsen, S. T. *J. Mater. Chem. C.* **2015**, *3*, 2528–2538.

(2) Zhao, H. B.; Zhang, Y. Y.; Bradford, P. D.; Zhou, Q. A.; Jia, Q. X.; Yuan, F. G.; Zhu, Y. T. *Nanotechnology* **2010**, *21*.

(3) Lipomi, D. J.; Vosgueritchian, M.; Tee, B. C. K.; Hellstrom, S. L.; Lee, J. A.; Fox, C. H.; Bao, Z. N. *Nat. Nanotechnol* **2011**, *6*, 788–792.

(4) Liu, Z. Y.; Qi, D. P.; Guo, P. Z.; Liu, Y.; Zhu, B. W.; Yang, H.; Liu, Y. Q.; Li, B.; Zhang, C. G.; Yu, J. C.; Liedberg, B.; Chen, X. D. *Adv. Mater.* **2015**, *27*, 6230–6237.

(5) Yamada, T.; Hayamizu, Y.; Yamamoto, Y.; Yomogida, Y.; Izadi-Najafabadi, A.; Futaba, D. N.; Hata, K. *Nat. Nanotechnol.* **2011**, *6*, 296–301.

(6) Seo, J.; Lee, T. J.; Lim, C.; Lee, S.; Rui, C.; Ann, D.; Lee, S. B.; Lee, H. *Small* **2015**, *11*, 2990–2994.

(7) Roh, E.; Hwang, B. U.; Kim, D.; Kim, B. Y.; Lee, N. E. *ACS. Nano.* **2015**, *9*, 6252–6261.

(8) Rahimi, R.; Ochoa, M.; Yu, W. Y.; Ziaie, B. *ACS. Appl. Mater. Interfaces* **2015**, *7*, 4463–4470.

(9) Ryu, S.; Chou, J. B.; Lee, K.; Lee, D.; Hong, S. H.; Zhao, R.; Lee, H.; Kim, S. G. *Adv. Mater.* **2015**, *27*, 3250–3255.

(10) Amjadi, M.; Pichitpajongkit, A.; Lee, S.; Ryu, S.; Park, I. *ACS. Nano.* **2014**, *8*, 5154–5163.

(11) Kim, K. K.; Hong, S.; Cho, H. M.; Lee, J.; Suh, Y. D.; Ham, J.; Ko, S. H. *Nano. Lett.* **2015**, *15*, 5240–5247.

(12) Cheng, Y.; R., W.; J., S.; Gao, L. *Adv. Mater.* **2015**, *27*, 7365–7371.

(13) Jeong, Y. R.; Park, H.; Jin, S. W.; Hong, S. Y.; Lee, S. S.; Ha, J. S. *Adv. Funct. Mater.* **2015**, *25*, 4228–4236.

(14) Kang, S.; Jones, A. R.; Moore, J. S.; White, S. R.; Sottos, N. R. *Adv. Funct. Mater.* **2014**, *24*, 2947–2956.

(15) Pang, C.; Lee, G. Y.; Kim, T. I.; Kim, S. M.; Kim, H. N.; Ahn, S. H.; Suh, K. Y. *Nat. Mater.* **2012**, *11*, 795–801.

(16) Lee, J.; Kim, S.; Lee, J.; Yang, D.; Park, B. C.; Ryu, S.; Park, I. *Nanoscale* **2014**, *6*, 11932–11939.

(17) Liao, X. Q.; Liao, Q. L.; Yan, X. Q.; Liang, Q. J.; Si, H. N.; Li, M. H.; Wu, H. L.; Cao, S. Y.; Zhang, Y. *Adv Funct Mater* **2015**, *25*, 2395–2401.

(18) Ge, J.; Sun, L.; Zhang, F. R.; Zhang, Y.; Shi, L. A.; Zhao, H. Y.; Zhu, H. W.; Jiang, H. L.; Yu, S. H. *Adv. Mater.* **2016**, *28*, 722–728.